SPH-Based FSI Simulations of Blood Flow in Patient-Specific Vessels with Deformable Walls

Chenxi Zhao & Oskar J. Haidn
Chair of Space Propulsion and Mobility
Technical University of Munich
Munich, Germany
chenxi.zhao@tum.de

Dong Wu & Xiangyu Hu
Chair of Aerodynamics and Fluid Mechanics
Technical University of Munich
Munich, Germany
xiangyu.hu@tum.de

I. Introduction

Cardiovascular diseases remain the leading cause of mortality worldwide as highlighted by the World Health Organization. In recent years, numerical simulations have become powerful tools for analyzing hemodynamics and vessel deformations, offering faster and non-invasive alternatives to experimental approaches. Fluid-structure interaction (FSI) modeling is particularly valuable, as it enables advanced research into cardiovascular diseases. Previous studies, such as those of Figueroa et al. [1] and Roy et al. [2], have shown the importance of vessel wall deformability in hemodynamic metrics like flow waveforms, wall shear stress and oscillatory shear index.

Current mesh-based methods for simulating blood flow in deformable vessels can be categorized into two main approaches: (1) frequent updates to the fluid and structural mesh geometry using formulations such as the Arbitrary Lagrangian-Eulerian (ALE) method, and (2) direct incorporation of vessel wall boundary effects into fluid equations, such as in the coupled momentum method (CMM). Although the ALE method yields accurate results, frequent mesh updates increase computational costs. Methods like CMM struggle to the accuracy with large deformable geometries, limiting its applicability [1]. On the other hand, Mesh-free methods, such as the smoothed particle hydrodynamics (SPH) approach, have gained attention in cardiovascular problems for overcoming challenges related to fluid-structure interfaces without requiring explicit interface-tracking techniques [3]. For example, Lu et al. [4] developed a 3D ISPH-TLSPH (incompressible SPH-total lagrangian SPH) framework that accurately modeled blood flow in thick-walled vessels, with results comparable to commercial cardiovascular software. However, the SPH method requires a kernel support region at least three times the largest particle spacing, which introduces modeling distortion in wall thickness and significant computational costs. To address this, thin structures can be represented as shells using a single layer of particles, an approach shown to enhance computational efficiency in solid mechanics simulations [5].

Accurate boundary conditions are equally critical in hemodynamics simulations. The inlet velocity profiles, such as plug flow or parabolic flow, significantly affect the value of time-averaged wall shear stress as shown in [6]. Besides, outlet boundary conditions, including constant pressure, resistance model, impedance model, and Windkessel (RCR) model, have been shown to yield distinct blood velocity and pressure fields [1], [7].

In this study, we present a comprehensive process for SPH-based simulations in vessels using SPHinXsys (an open-source library, https://github.com/Xiangyu-Hu/SPHinXsys). A general particle generation method is proposed for constructing wall and shell elements directly from standard triangle language (STL) and visualization toolkit (VTP) files. Then, we systematically evaluate the performance of wall-based and shell-based boundaries as well as their interactions with fluid. Furthermore, we impose different outlet pressure boundary conditions and compare the results with mesh-based methods. Finally, the proposed methodology is applied to two clinically relevant cases, i.e. the carotid artery and the aorta, demonstrating its versatility and robustness in modeling FSI processes in deformable vessels.

II. Methodology

A. Particle generation for wall and shell boundaries

The geometry of cardiovascular structures is typically provided in STL or VTP format. To construct vessel wall geometries from these existing STL/VTP blood flow files, a typical approach involves suturing the triangular surfaces and extending the integral surface with a specified thickness in the 3D design software. However, this process is challenging and may result in suboptimal wall geometry quality. Furthermore, predicting the wall thickness during the modeling phase can limit the flexibility to explore resolution-dependent effects during simulations. To address these challenges, we directly generate wall and shell particles with the thickness property in the SPH framework using the input blood flow geometry files.

The vessel wall or shell geometry is constructed using an extrusion method based on the STL triangle mesh of the blood flow geometry in Fig.1(a) and Fig.2(a). The thickness of the solid is defined as a multiple of the initial particle spacing dp_0 ($4dp_0$ for wall boundary in Fig.1(b); dp_0 for shell boundary in Fig.2(b)). This approach constructs a completely enclosed vessel wall geometry, whose sealed inlet and outlet need to be further

processed.

For the wall particle generation, a lattice distribution of particles is initially generated within the domain of the wall geometry in Fig.1(c). The particle positions are then refined using a physics-driven relaxation method combined with surface bounding techniques, as described in [8]. To handle the sealed inlet and outlet regions, rectangular boxes with a length and width exceeding the vessel width and a height of $4dp_0$ are placed at the inlet and outlet. After the relaxation process is complete, all wall particles are identified, and the particles located within the boxes are removed. These removed particles are excluded from the final particle data saved in the reload file, as shown in Fig.1(d), which is used in physical simulations.

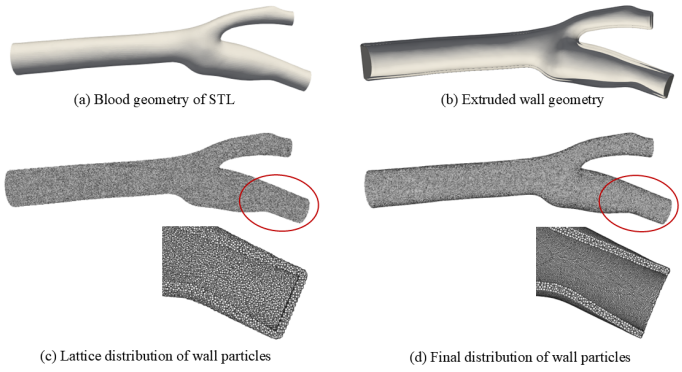

Fig. 1. Illustration of wall particle generation.

For the shell particle generation, the total number of shell particles to be positioned on the surface is calculated as:

$$N = \lceil \frac{area_{\text{STL}}}{dp_0^2} \rceil, \tag{1}$$

where $area_{\text{STL}}$ represents the total surface area of the STL or VTP geometry. The number of particles assigned to each triangular face of the mesh is determined based on the proportion of the face area to the total mesh area. Within each selected face, the particle positions are evenly distributed relative to the triangle's vertices, as depicted in Fig.2(c). Then, the bounding method for surface relaxation constrains shell particles directly onto the geometry surface by identifying the closest points on the surface. Additionally, particle normals are smoothed within their support domain following the approach proposed in [9]. After the relaxation process, the inlet and outlet particles for the shell boundary are removed using the same box detection method as in wall particle generation, as shown in Fig.2(d).

B. Fluid-structure interaction equations in SPH discretization

In this study, blood is modeled as a weakly compressible Newtonian viscous fluid. The pressure is calculated using an artificial equation of state:

$$p = c^2(\rho - \rho_0), c = 10V_{\max}, \tag{2}$$

where c is the numerical sound speed. The SPH discretization of continuity and momentum equations with a low-dissipation

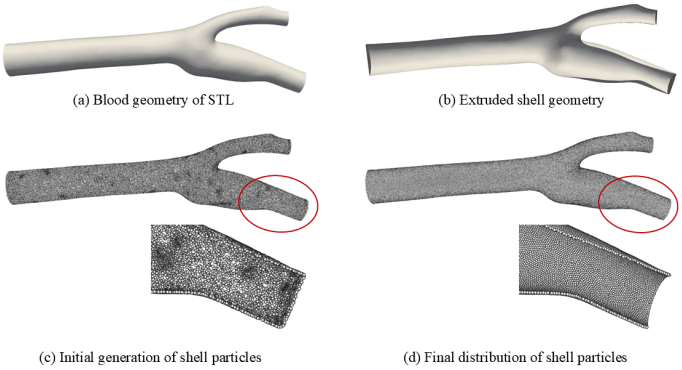

Fig. 2. Illustration of shell particle generation.

Riemann solver for the hemodynamics can be written as

$$\frac{\mathrm{d}\rho_i}{\mathrm{d}t} = 2\rho_i \sum_j \frac{m_j}{\rho_j}(\mathbf{v}_i - \mathbf{v}^*) \cdot \nabla_i W_{ij}, \tag{3}$$

$$\frac{\mathrm{d}\mathbf{v}_i}{\mathrm{d}t} = -2\sum_j m_j \frac{p^*}{\rho_i \rho_j}\nabla_i W_{ij} + 2\sum_j m_j \frac{\eta_{ij}}{\rho_i \rho_j}\frac{\mathbf{v}_{ij}}{r_{ij}}\frac{\partial W_{ij}}{\partial r_{ij}} + \mathbf{f}_i^{s:p} + \mathbf{f}_i^{s:\nu}. \tag{4}$$

For solid mechanics, the total Lagrangian formulation is employed. The density and momentum equations are

$$\rho_i = \rho^0 \frac{1}{\det(\mathbb{F})}, \tag{5}$$

$$\frac{\mathrm{d}\mathbf{v}_a}{\mathrm{d}t} = \sum_b \frac{m_b}{\rho_a \rho_b}(\mathbb{P}_a \mathbb{B}_a^0 + \mathbb{P}_b \mathbb{B}_b^0)\nabla_a^0 W_{ab} + \mathbf{f}_a^{f:p} + \mathbf{f}_a^{f:\nu}. \tag{6}$$

Here, subscript a refers to a solid particle. $\mathbb{B}_a^0$ is the correction matrix for spatial homogeneity, and $\mathbb{F}$ is the deformation tensor.

The smoothing length for fluid and solid discretization are expressed as h_f and h_s, and $h_f \geq h_s$. For this study, $h_f = 1.3\Delta x$ and $h_s = 1.15\Delta x$, where Δx is the initial particle spacing. The forces exerted by the solid walls on the fluid are integrated into the fluid's momentum equation, and the forces exerted by the fluid on the solid walls are equal and opposite:

$$\mathbf{f}_i^{s:p}(h_f) = -2\sum_a m_a \frac{p^*}{\rho_i \rho_a}\nabla_i W(\mathbf{r}_{ia}, h_f), \tag{7}$$

$$\mathbf{f}_i^{s:\nu}(h_f) = 2\sum_a m_a \frac{\eta_{ia}}{\rho_i \rho_a}\frac{\mathbf{v}_i - \mathbf{v}_a^d}{|\mathbf{r}_{ia}| + 0.01h}\frac{\partial W(\mathbf{r}_{ia}, h_f)}{\partial r_{ia}}. \tag{8}$$

The fluid-shell interaction follows similar principles but with specialized formulations. These details, part of ongoing research, will be published in the near future work.

C. Inlet and outlet boundary condition implementation

To impose velocity and pressure boundary conditions at the inlet and outlet(s), we adopt the four-layer bidirectional buffer approach proposed in [10]. At the inlet, a time-dependent velocity profile is imposed, while at the outlet(s), various pressure boundary conditions including constant pressure, resistance model, and Windkessel model are implemented.

For the resistance model, the outlet pressure is determined as

$$p = p_0 + QR, \tag{9}$$

where p_0 is the base pressure, Q is the outlet flow rate and R is the resistance parameter.

For the Windkessel model, the outlet pressure is governed by the following ordinary differential equation (ODE):

$$\frac{\mathrm{d}p}{\mathrm{d}t} + \frac{p}{CR_d} = \frac{R_p + R_d}{CR_d}Q + R_p\frac{\mathrm{d}Q}{\mathrm{d}t}, \tag{10}$$

where R_p and R_d are the proximal and distal resistances, respectively, and C is the vascular compliance. The estimation of the RCR parameters is based on the principle outlined in [11].

The flow rate Q in the above two equations is calculated as an average value over a predefined time period to ensure simulation stability, instead of using the transient flow rate. The pressure in (10) is solved using a modified Euler's method, as described in [4], ensuring numerical stability and precision in the simulations.

III. Results and Discussion

This section presents a part of the results and findings of this study.

Fig.3 presents the hemodynamic simulation results for the carotid artery under two boundary conditions: wall boundary and shell boundary. The velocity fields exhibit similar patterns at identical time points, while the shell boundary approach significantly reduces computational time, underscoring its efficiency.

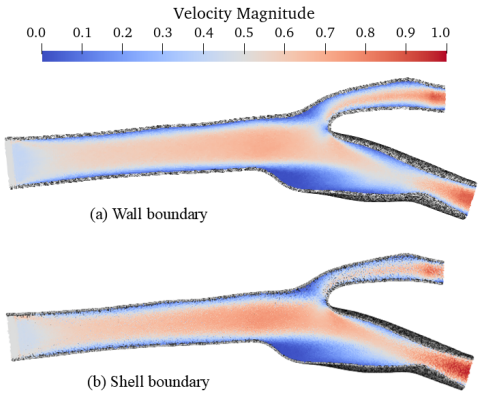

Fig. 3. Hemodynamics simulations of the carotid artery with velocity inlet and constant pressure outlet.

Fig.4 illustrates the fluid-shell interaction results for the carotid artery, including the velocity field of the blood flow and the corresponding stress and deformation of the shell induced by hydrodynamic forces.

IV. Conclusion

This study presents a comprehensive approach for SPH-based simulations of fluid-structure interactions in vessels. A general particle generation method is introduced to construct wall and shell elements directly from VTP and STL files, streamlining the modeling process. The comparative analysis of wall-based and shell-based boundaries for hemodynamic simulations is conducted. Additionally, the effects of varying outlet pressure boundary conditions are systematically examined. The proposed methodology is further validated through fluid-shell interaction simulations within the carotid artery, demonstrating its capability in patient-specific vessels.

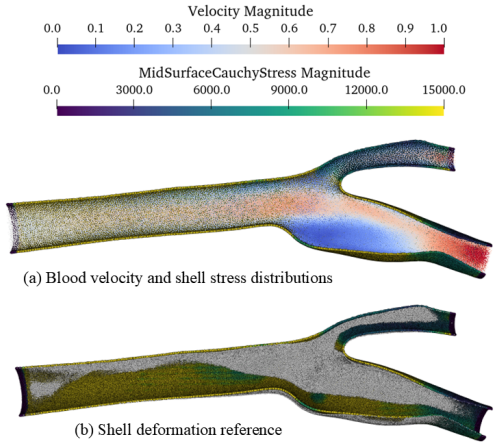

Fig. 4. Fluid-shell interaction of carotid artery with velocity inlet and constant pressure outlet.

References

[1] C. A. Figueroa, I. E. Vignon-Clementel, K. E. Jansen, T. J. Hughes and C. A. Taylor, "A coupled momentum method for modeling blood flow in three-dimensional deformable arteries," *Computer Methods in Applied Mechanics and Engineering*, vol. 195, pp. 41-43, 2006.

[2] M. Roy and C. Suman, "How does the stiffness of blood vessel walls and deposited plaques impact coronary artery diseases?," *Physics of Fluids*, vol. 36.8, 2024.

[3] S. Laha, G. Fourtakas, P. K. Das and A. Keshmiri, "Smoothed particle hydrodynamics based FSI simulation of the native and mechanical heart valves in a patient-specific aortic model," *Scientific Reports*, vol. 14(1), 6762, 2024.

[4] Y. Lu, P. S. Wu, M. B. Liu and C. Zhu, "A GPU-accelerated 3D ISPH-TLSPH framework for patient-specific simulations of cardiovascular fluid–structure interactions," *Computer Methods in Applied Mechanics and Engineering*, vol. 428, 117110, 2024.

[5] D. Wu, C. Zhang and X. Y. Hu, "An SPH formulation for general plate and shell structures with finite deformation and large rotation," *Journal of Computational Physics*, vol. 510, 113113, 2024.

[6] S. Madhavan and E. M. C Kemmerling, "The effect of inlet and outlet boundary conditions in image-based CFD modeling of aortic flow," *Biomedical engineering online*, vol. 17, pp. 1-20, 2018.

[7] I. E. Vignon-Clementel and C. A. Taylor, "Outflow boundary conditions for one-dimensional finite element modeling of blood flow and pressure waves in arteries," *Wave Motion*, vol. 39(4), pp. 361-374, 2004.

[8] Y. J. Zhu, C. Zhang, Y. C. Yu and X. Y. Hu, "A CAD-compatible body-fitted particle generator for arbitrarily complex geometry and its application to wave-structure interaction," *Journal of Hydrodynamics*, vol. 33(2), pp. 195-206, 2021.

[9] D. Wu, Y. C. Yu, C. Zhang, X. Y. Hu and B. Rochlitz, "Level-set based mid-surface particle generator for thin structures," 17th SPHERIC World Conference, 2023.

[10] S. G. Zhang, Y. Fan, Y. R. Ren, B. Qian and X. Y. Hu, "Generalized and high-efficiency arbitrary-positioned buffer for smoothed particle hydrodynamics," *Physics of Fluids*, vol. 36(12), 2024.

[11] A. Deyranlou, J. H. Naish, C. A. Miller, A. Revell and A. Keshmiri, "Numerical study of atrial fibrillation effects on flow distribution in aortic circulation," *Annals of biomedical engineering*, vol. 48, pp. 1291-1308, 2020.